PROJECT FINAL REPORT

Grant Agreement number: 256984

Project acronym: ENDOTOFPET-US

Project title: Novel multimodal endoscopic probes for simultaneous PET/ultrasound imaging for image-guided interventions

Funding Scheme: Small or medium-scale focused research project

Period covered: from January 1st, 2011 to June 30th, 2015

Name of the scientific representative of the project's co-ordinator[1], Title and Organisation:

Prof. René Laugier UNIVERSITE D'AIX MARSEILLE

Tel: +33 4 91 38 60 23

Fax: +33 4 91 38 48 73

E-mail: rlaugier@ap-hm.fr

Project website address: http://endotofpet-us.web.cern.ch/endotofpet-us/

[1] Usually the contact person of the coordinator as specified in Art. 8.1. of the Grant Agreement.

4.1 Final publishable summary report

4.1.1 Executive summary

The ENDOTOFPET-US project aims at developing new cancer biomarkers with a specific focus on prostatic and pancreatic cancers, entities with almost asymptomatic development and, in the case of pancreatic cancer, very bad prognosis if not detected and treated eraly.

A new, higher performance imaging tool with multimodal capability has been developed in the frame of this project, introducing breakthrough technologies for novel endoscopic procedures in diagnostic and therapeutic endoscopy and in surgical oncology aiming at diagnosing more patients with earlier tumour stages and improving patient outcome and therapy, as well as reducing health costs. The system aims at a very high sensitivity allowed by the endoscopic approach and the proximity of the target, a spatial resolution of 1mm to delineate early tumors, and a time resolution of 200ps to reject by time-of-flight techniques the high background due to the other organs, as this is the first time part of a PET system is inside the patient.

The system consists of a miniaturized PET head installed on a commercial ultrasound endoscope and an outer PET plate placed outside the body in coincidence with the PET head (Fig. 1).

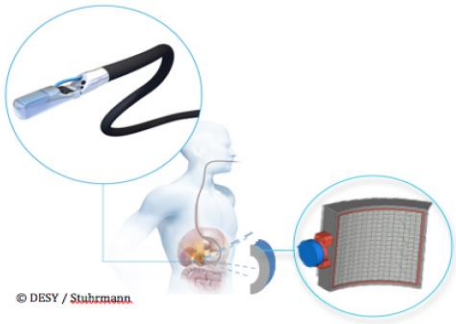

Fig. 1. The EndoTOFPET-US detector system sketched in the application for pancreatic cancer diagnostics. Top left is the rendering of the ultrasound endoscope with PET extension, which needs to be positioned inside the stomach below the pancreas. Bottom right is the external plate detector positioned outside the body on the opposite position to the endoscope with respect to the pancreas.

The two detectors need to be positioned with respect to each other to a precision of better than a millimeter for the duration of the examination. This task is performed by a combination of optic and electromagnetic tracking systems. Each of the two detectors consists of LYSO inorganic scintillators to convert the 511keV photons from positron-electron annihilation to scintillation light. The crystals are coupled one-to-one to blue-sensitive photo-detectors optimized for ultimate timing resolution. The signals of the photo-detectors are digitized either in the photo-detectors itself (with a multi-digital pixellated photodetector developed specifically for this project), or via additional off-detector electronics for the external plate. The system is controlled by an off-detector data acquisition and slow control system. The compact data acquisition system handles rates up to 40 MHz from the external plate and 200 kHz from the internal probe. Specific programmable circuits (FPGA) on the front-end boards concentrate the event data from the external plate and transmit it to an external trigger. The data acquisition card then merges these data with the one from the internal probe allowing a selection of coincidence events.

Two versions of this device have been built, one for the prostate and one for the pancreas. Preclinical tests have been conducted on pigs with the prostate version and have led to very encouraging results. The system is now ready for systematic investigations of new and very promising biomarkers, such as ^{68}Ga-PSMA and ^{68}Ga-Bombesin for the prostate and a new antibody developed by one partner of the consortium for the pancreas (16D10 glycosylated antigen).

The project documentation is continuously updated on a web site with public and private sections (http://endotofpet-us.web.cern.ch/).

4.1.2 Summary description of the project context and main objectives

Concept and clinical objectives

The main clinical objective is to address image-guided diagnosis and minimally invasive surgery with a miniaturized bimodal endoscopic probe with a millimetre spatial resolution and a significantly higher sensitivity than whole-body PET scanners. The aim is to improve harvesting of tumoral tissue during biopsy by combining the functional biological information of radioactive biomarkers with the morphological information obtained from ulrasound (US). A first stage of preclinical investigations on pigs have paved the way for clinical investigations in the 3 hospitals of the consortium.

Surgery has undergone several paradigm changes in the last century, and minimally invasive surgery techniques are now considered state of the art. Identically, flexible endoscopy is now the primary tool used in gastroenterology, which has evolved into a well-accepted and initial diagnostic or therapeutic intervention in a variety of diseases, especially in premalignant or malignant lesions of the entire gut. Coupled with conventional endosonography, the proposed probe will dramatically improve the detection capacity of early cancers and precise diagnosis of small lesions or tumours, but also characterization in terms of histology (endocrine tumours, discrimination between benign and malignant lesions, etc.). Therapeutic endoscopy allows removing early cancers, without any skin incision: more and more attention is turned toward natural orifice transluminal endoscopic surgery (NOTES), which involves accessing the peritoneal cavity through one of the body's natural orifices avoiding the need for abdominal incision or laparoscopic surgery (SILS). The ability to attach a miniaturized PET detector to an endoscopic ultrasound probe close to intra-abdominal tumours drastically increases the sensitivity of detecting smaller tumours and allows directing tissue sampling with fine needle biopsy under anatomic and functional image guidance as provided by the fused PET-US images.

The proposed approach will bring significant improvements over conventional laparoscopy, such as the absence/minimization of body scar, decreased stress and postoperative pain, shorter hospitalization or even outpatient setting, smaller complication rate such as adhesions or infections, decreased postoperative inflammation and less immuno-suppression, as well as reduced treatment costs.

Moreover it will give the possibility to identify by endoscopy **biologic, functional markers (biomarkers)** and to map them to morphologic structures to precisely determine the extension of abnormal tissues, thus permitting endoscopic surgery with high precision. Finally, using this hybrid information to obtain tissue samples for histo-pathological analysis and the increased sensitivity provided by this instrument, will improve the use of **actual biomarkers** of tumoral processes such as metabolism (^{18}F-fluorodeoxyglucose), proliferation (^{18}F-fluorothymidine), angiogenesis (^{18}F-galacto-RGD), amino acid metabolism (^{18}F-fluoroethyltyrosine, ^{18}F-DOPA) or somatostatin receptor (^{68}Ga-DOTATOC). That will contribute to a better staging of the tumour and evaluation of development and dissemination of metastases, as well as response to therapy. Furthermore, this new instrument will help evaluating **novel preclinical and clinical biomarkers** by allowing precise histo-pathological correlations between tissue sampling and imaging features.

Technical design and objectives

It was proposed to build a PET-US endoscopic probe around a commercial US assisted biopsy endoscope. The PET detector head is a small array of 700 micron diameter heavy Lutetium-Yttrium orthosilicate scintillating crystals (LYSO) readout by novel ultrafast and low bias (<30V) photo-detector array based on Geiger mode avalanche photodiodes. In close proximity to the organ under study (prostate, pancreas, lymphadenopathy or mediastinum) this detector head, even small, covers a large solid angle and provides a high sensitivity. Background rejection is obtained by electronic collimation on the few centimetres Region Of Interest (ROI) by high performance Time-of-Flight techniques between the endoscopic crystal head and an outer crystal array positioned external to the patient. The real time knowledge of the relative position of the two PET detector heads is provided by a sub-millimetre precision miniaturized optical (for the prostate) or magnetic (for the pancreas) tracking system.

This project relies on recent impressive progress in three technological areas (scintillator performances and production methods, light transport, photo-detectors) and integrates them in a small-sized highly miniaturized and fully digital endoscopic probe with unprecedented timing and spatial resolution.

This ambitious approach in the domain of non-invasive in-vivo image-guided diagnosis and minimally-invasive surgery relies on a number of objectives listed below.

a- The first objective was to build a detection head behaving as an optical photon counter and providing therefore a quantum detection scheme for photons over a wide spectral range (from visible to γ-rays) and a fully digital signal at the level of the photo-detector.

As a quantum detection head it will provide full access to the statistical information in the generation of the photons with the potential of accessing the ultimate timing resolution. The management of individual photons allows this detector head to work in a wide range of incident photons energies, covering not only the PET energy, but also SPECT, multispectral X-Rays, and even optical modalities. This is achieved by the use of a new generation of Geiger mode avalanche photo-detector (SPAD), which integrates SPAD array and readout electronics in the same silicon complementary metal–oxide–semiconductor (CMOS) die. Each SPAD can detect single optical photons with a high timing precision of a few tens of picoseconds.

b- A second objective was to reach a 200ps timing resolution, corresponding to a spatial resolution of 3 cm along the Line of Response (LOR) in a dual-head system, allowing a direct (and therefore fast) 3-dimensional reconstruction through a limited number of angular projections only, and an efficient rejection of background coming from outside of the few cubic centimetres region of interest (ROI).

The concept of quantum photon detector discussed in the previous paragraph was a prerequisite to reach a timing resolution of 200ps at the system level. Besides using the highly integrated photo-detector-electronics digital system described above it required additional efforts at the level of the scintillation light production in the crystal, and of the light transport to the photo-detector.

The time resolution of a scintillator-based detector is determined by the rate of photoelectrons at the detection threshold, which depends on the time distribution of photons arriving on the photo-

detector. It is then essential to develop scintillation materials with the highest light yield and a short rise and decay time.

Maximizing the light yield, and in particular the initial density of photons, while minimizing the rise and decay time, requires an optimization of the energy transfer mechanisms to the activator as well as to the energy transition type at the activator ion. The consortium benefited from a strong expertise on scintillating crystals and identified several scintillating crystals (LuAG:Ce, LuAG:Pr, LYSO:Ce, LuAP:Ce, LaBr3:Ce), as possible candidates. After a thorough investigation of the properties of these crystals and the possibility to optimize their performance for this application the choice has been made on cerium doped LYSO crystals., because of its excellent light yield as well as short rise time and decay time.

A particular emphasis has been put on the light transport within the crystal and on the efficiency of photon transfer to the photo-detector. Photons being emitted isotropic from the conversion point, the detector geometry had to be optimized to decrease the optical path-length to the photo-detector, reduce the light bouncing within the scintillator and improve the matching factor between the crystal and the photodetector.

c- A third objective was to achieve a millimetre spatial resolution for the PET detector head.

This requires a very fine segmentation of the endoscopic detector head. There is a less stringent requirement for the external PET detector plate, because of the magnification factor induced by the geometrical asymmetry of the PET system. The production of sub-millimetre section scintillating crystals is challenging. Several approaches were investigated in the frame of the project, including the Micro-Pulling-Down technique (MPD) developed by one company member of the consortium, to grow 20mm long scintillating fibres with a diameter of a few hundreds of microns. This was a prerequisite to build a very high granularity detector head, necessary to achieve the required spatial resolution of about 1mm within the organ under examination. Other more classical methods have also been investigated in parallel to produce these very fine pixels and assemble them in compact arrays providing good light collection efficiency, while minimizing the optical cross-talk between pixels.

d- A fourth objective was to integrate all the components in a very compact detector head with an efficient tracking system for a sub-millimetre on-line determination of the position of the different imaging parts.

Very precise and compact mechanical assembly was required at the level of the endoscopic detector head. In order to provide space for the readout electronics of each individual SPAD of the photodetector the sensitive area of the photodetector has to be reduced. Several solutions were studied to reclaim this reduced fill factor including by means of advance highly compact micro-optical elements such as micro-lenses or diffractive optics coupling films.

The endoscopic PET detector head had to be mounted in front of the US probe, with a small tilt angle in order to allow good overlap of the ROI coverage by both modalities. Of particular importance is the real time precise knowledge of the relative positioning of the PET endoscopic head and the outer plate. The consortium had to develop a very compact tracking system to record the 3 spatial coordinates in real time with a sub-millimetre resolution together with the 3 positioning angles.

Beside the hardware integration, real-time image fusion from the TOF-PET and US imaging modalities was developed in the frame of a dedicated detector integration work package.

Progress beyond the state-of-the-art

The ability to place a PET detector very close to tumour tissue with increase radiopharmaceutical uptake leads to detect considerably smaller amounts of tumour tissue than is currently achievable with state-of-the-art PET scanners (a few mm^3 instead of 0.3–$1cm^3$) potentially allowing to detect micro-metastases or micro-lesions, to help histological characterization and to allow endoscopic destruction or resection.

With its high background rejection power, full imaging capability with unprecedented sensitivity and spatial resolution and bimodal imaging approach the TOF-PET-US endoscopic probe allows a millimetre determination of the tumour foci and tumour margins.

Present intra-operative and endoscopic imaging systems are limited in their potential to precisely determine the tumour margins and the number and precise localization of tumour foci and include no functional imaging information. Bimodal imaging opens unprecedented capabilities to realize biopsies guided by functional imaging in real-time, by visualizing the markers of tumour biology (PET) superimposed to the morphologic information obtained by endosonography. This allows following the advancement and placement of a tool (biopsy or radiofrequency needle, etc.) in the desired functional imaging characteristics of the tumour to sample/resect, such as increased metabolism, proliferation, angiogenesis and apoptosis.

With an objective of 200ps timing resolution, a spatial resolution of 3cm is achievable along the LOR, allowing the localization of the organ under examination (for instance the prostate, the pancreas or a lymph-node) in a direct and fast way, without the need for cumbersome and time consuming iterative or back-projection algorithms. All commercial PET cameras are not using the Time-of-Flight information and are limited in timing resolution at the level of about 2ns. Recently there has been a renewal of interest for TOF-PET systems in relation with the development of fast and high light yield crystals, such as LSO :Ce. A few commercial PET camera are now available with a timing resolution of about 600 picoseconds, corresponding to a spatial resolution along the LOR of approximately 9cm, which helps reducing the difference in image quality between slim and fat patients but does not yet allow direct 3D reconstruction of small and medium size organs.

Applied to whole body PET scanners and for an equivalent image quality a dose reduction by a factor 3 to 10 can therefore be expected as compared to state-of-the-art technology or the acquisition time can be reduced accordingly, leading to higher patient throughput, better patient comfort and smaller impact of moving tissues on image quality. The improvement in the timing performance by a factor of 3 (compared to the 2 recent TOF-PET machines) and up to 10 (compared to the majority of commercially available non TOT-PET machines) results in an increase by the same factor in the image signal-to-noise (S/N) ratio. This improvement can be exploited to conduct faster exams and/or to reduce the doses to the patient. This last point is of particular importance in a context of increased concern about patient and medical personnel radiation exposure. In fact, even if the full dose reduction is applied the image quality is still expected to improve as the random coincidences rate is decreasing as the square of the dose.

4.1.3 Description of the main S&T results/foregrounds

In the frame of this ambitious project a number of challenges have been addressed, both technically and clinically, which have led to the development and introduction of cutting edge technologies. This has been the tasks of different workpackages regrouping the competences and expertise in the different scientific domains concerned.

WP2: Crystals and optics

a) Crystal selection

The time resolution of a scintillator-based detection system such as the one used in our project is determined by the rate of photoelectrons at the detection threshold, which depends on the time distribution of photons being converted in the photodetector. Therefore the main crystal parameters influencing the time resolution of a scintillator detector are the light yield , the scintillation rise time and decay time. In order to identify the most appropriate crystal for the project, various types of crystals have been evaluated in terms of light yield (LY) and coincidence time resolution (CTR) [1].

Based on a survey of existing scintillators, we have evaluated two different types of lutetium-based crystals with the most appropriate features for our application:

- Lutetium ortho-silicates such as Lu_2SiO_5 (LSO) and its derivatives such as LYSO, or LGSO, in which part of the lutetium atoms are replaced by yttrium or gadolinium atoms, respectively. These scintillators are dense ($\leq$7.4g/cm^3) and, if doped with cerium, have a decay time of approximately 40ns and a fairly high light output ($\geq$ 20'000 Ph/MeV);
- Lutetium aluminum garnets, $Lu_3Al_5O_{12}$ (LuAG). LuAG has a density of 6.73g/cm^3 and, when doped with praseodymium, a light emission decay time of about ~20ns.

Based on the comparison of light yield of LuAG:Ce, LuAG:Pr and LYSO:Ce and on the coincidence time resolution measurements in [1], **the decision was taken to choose LSO or LYSO crystals as the baseline scintillator for the EndoTOFPET-US project** [2]**.** In the end, this choice proved to be highly viable as the project achieved a CTR of 238ps FWHM with LYSO scintillators of a pixel size of 0.71 x 0.71 x 10 mm^3 (internal probe specification) in coincidence with LYSO crystals of 3 x 3 x 15 mm^3 size (external PET panel or plate specification). It should be noted that the achieved value, shown in Fig. 1, is very close to the targeted value of 200ps.

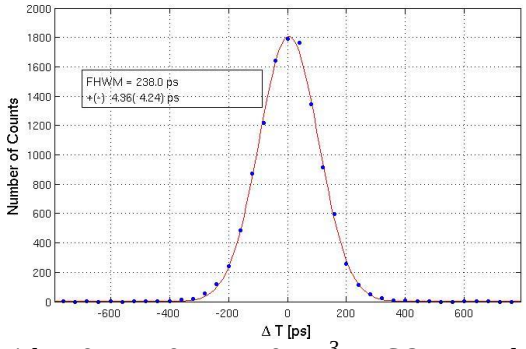

Fig 1: Delay time spectrum with a 0.71 x 0.71 x 10mm^3 LYSO crystal (internal probe) in coincidence with a LYSO crystal of 3 x 3 x 15mm^3 (external plate) to determine the coincidence time resolution (CTR).

b) Comparison and selection of production methods for scintillating crystals

In order to achieve a spatial resolution of less than 1mm for the internal probe, scintillating crystals of sub-millimeter cross section of the order of 0.7 x 0.7 mm^2 are required. The production of such

'fibers', using standard crystal production techniques, is expensive because of the delicate cutting and polishing processes. By using a new technique called "Micro Pulling Down" (µPD), developed by Fibercryst (a company of the consortium), the cost of mechanical processing could substantially be reduced. This new technique was quite challenging, and many obstacles such as cracks, uncontrolled geometry deviations, radial and lateral segregation of the dopant have to be overcome to obtain reproducible, high quality crystals needed for our project. During the first 24 months of the project, intensive work was invested in the optimization of the crucible shapes and the parameters for crystal growing of LYSO:Ce and LuAG:Ce fibers. Despite the extensive progress made in this area, the final evaluation of this technique concluded that the production of such fibers was still immature to produce these scintillators with sufficient quality in time for the EndoTOFPET-US project.

Consequently, in M24 the decision was taken to use, in the framework of this project, pixel crystals produced from bulk material and not crystals made with the micro-pulling-down technique.

Nevertheless the work on µPD-fiber production continued during the second period of the project where further progress was made, in particular, on LuAG:Ce fibers, i.e. in terms of surface quality, dopant segregation, reproducibility and light attenuation (see Figs. 2, 3) [3]**.**

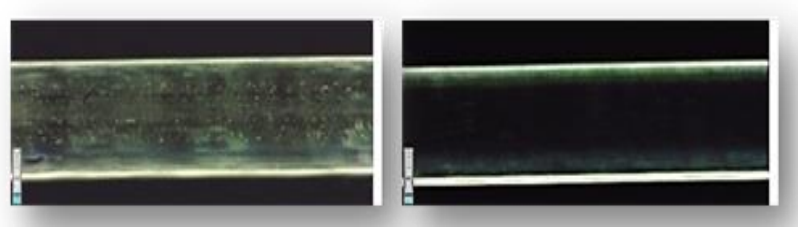

Fig. 2: 2mm diameter Ce:LuAG fibers; left: with high Ce concentration; right: with low Ce concentration

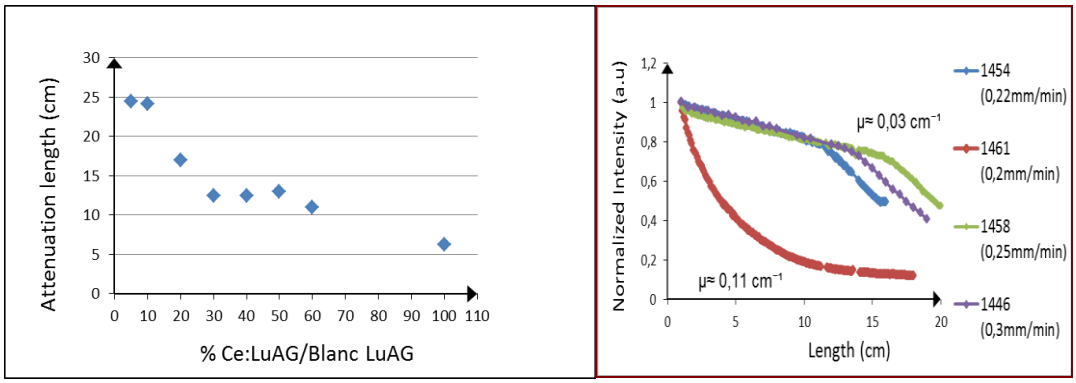

Fig. 3: 2mm diameter Ce:LuAG fibers; left: attenuation length vs. cerium content; right: light attenuation for different growth rates.

In view of the inherent difficulties associated with the micro-pull-down growth of ortho-silicate crystal fibers – Fig. 4 illustrates the problematic of growing homogeneous crystals with adequate mechanical and optical quality – development work continues with the following perspectives:

- One of the next tasks is to optimize the growing atmosphere in order to maintain the stoichiometry of the YSO matrix, avoid iridium particle deposition, and enhance fiber hardness.
- Another objective is to study and apply annealing processes to improve fiber hardness unless atmosphere optimization (above) already solves that problem to begin with.
- Thirdly, it is foreseen to add cerium to the compound and pull several samples at different cerium concentrations before gradually adding lutetium to the YSO matrix. One can then

proceed trying different stoichiometry values of yttrium and lutetium in order to find the best compromise between optical quality and luminescence.

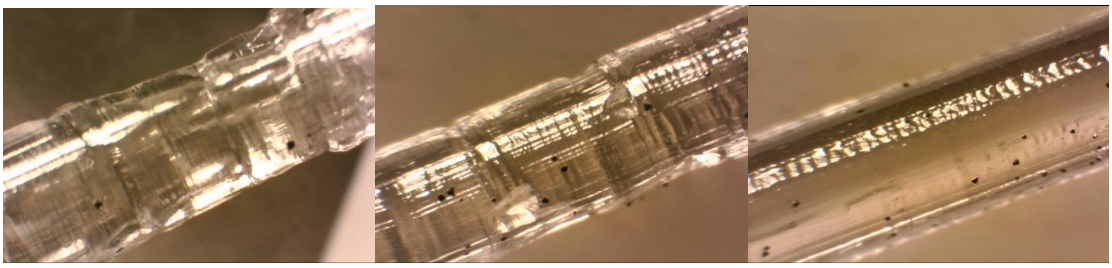

Fig. 4: 1.2mm diameter YSO fibers: Left to Right shows the quality improvement during the study, changing different parameters.

This work on the optimization of the µPD technique, even if not chosen for the EndoTOFPET-US project, has led to a better understanding of the key parameters applicable for this process. It should be noted that the "RISE" European project (Intelum), involving CERN, Milano and Fibercryst, was launched to follow up on this work and develop such fibers for high energy physics [4].

c) Crystal matrices: production and evaluation

Once the choice of crystal type and production was made, the manufacture of the matrices for both the internal probe and the external plate was authorized, and consequently all matrices produced on schedule. For the *internal* detector, several matrices of 9 x 18 LYSO crystals from the company Proteus with a cross section of 700µm and lengths from 8 to 15mm were produced [5]. On the other hand, for the *external* plate (note: in the end two such plates were built) 276 matrices of 3.5 x 3.5 x 15mm^3 crystals (first plate) and 276 matrices of 3.1 x 3.1 x 15mm^3 (second plate) were furnished by the company CPI. Note, that the crystal cross section is different for the two plates as the size of the MPPC photodetector array (WP3) has changed for the second plate. Fig. 5 shows five crystal matrices for the internal probes, whereas Fig. 6 shows a large set of matrices for the external plate.

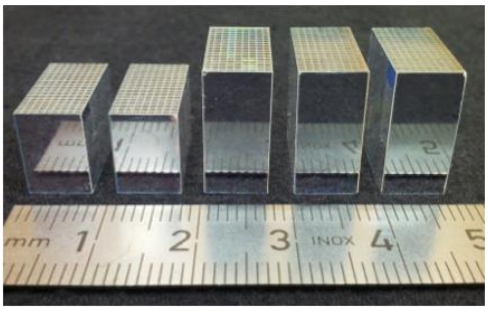

Fig. 5: Five crystal matrices for the internal probe

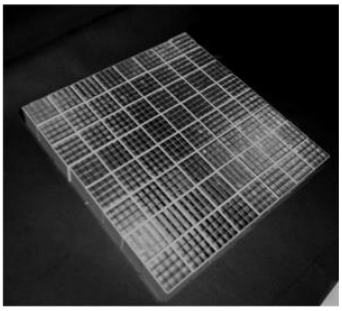

Fig. 6: Set of assembled matrices for the ext. plate

As to the crystal reflectors, an enhanced specular reflector film "ESR" made by 3M [6] was selected. Compared to other reflecting materials such as e.g. $BaSO_4$-paint or Tyvek (both >150µm thick for similar performance results), 3M's ESR is significantly thinner (~80µm) and thus more favorable in terms of dead space between pixels, which is now reduced to less than 100µm. This is particularly important for the internal probe with its very small sensitive volume.

All matrices were visually inspected at CERN and subsequently characterized in terms of size and LY. The characteristics of each matrix are stored in a database specially developed for the project.

For both type of matrices (internal probe and external plate), the LY obtained is largely above 20'000ph/MeV, formerly specified as the minimum required to achieve adequate time resolution. An average value of 24'000ph/MeV was found for the matrices of the internal probes, whereas for the two external plates the average value (calculated from 276 matrices) was 32'700ph/MeV and 36'700ph/MeV, respectively. Fig. 7 shows the LY distributions for the crystal matrices of the two external plates.

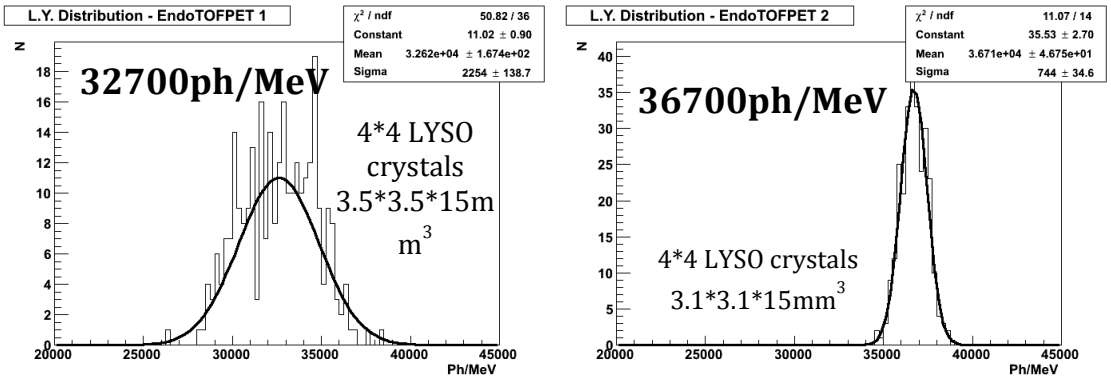

Fig. 7: LY distribution of the 276 matrices of the 1st plate (left); LY distr. of the 276 matrices of the 2nd plate (right)

After its evaluation, the crystal matrix was coupled to a MPPC array to build a crystal "module". These modules were subsequently mounted on the body of the external plate. A special assembly bench was designed and built at CERN to glue the crystal matrices to the MPPC arrays with very high precision [2]. After the gluing of the matrices and the MPPC arrays a measurement of the CTR was made for each such module [7,8], a suitable method to check their functionality. This was done with a dedicated test bench setup at CERN [7,8] where we apply the time-over-threshold technique together with the ultra-fast amplifier-discriminator chip NINO [9] and a fast TDC (HPTDC) [10]. Fig. 8 shows histograms of the CTR from each channel of the modules of the two plates. **For both plates the CTR values measured for each module are close to our target figure of 200ps FWHM.**

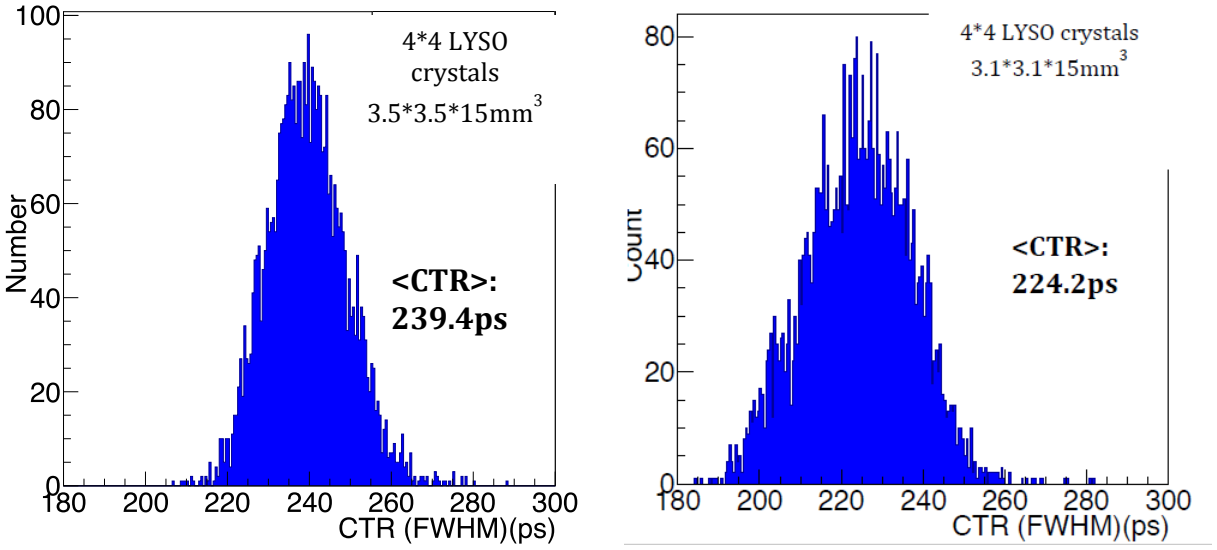

Fig. 8: CTR distributions of the crystal modules for the first (left) and second plate (right)

3. Light transport and optical coupling to the photodetector

Due to the low fill factor of ~50% of the *digital* SiPM used as the photodetector of the internal probe and, hence, in order to maximize the amount of light impinging on the active area of the photodetector, we initially proposed to insert a light focusing or so called micro-optical-element (MOE) between the crystal array and *digital* SiPM. This element was meant to focus the light onto the *active* areas (SPADs) of the photodetector only and then, to some extent, compensate for the light losses caused by the *insensitive* zones of the photodetector. The idea was to define the best possible MOE configuration and consequently to combine crystal, MOE and the SPAD arrays of the *digital* SiPM in such way that a maximum of light reaches the active areas of the photodetector. Several approaches were studied, both via simulation and experiment: micro-prism-concentrators, micro-lens- collimators coupled to a light extractor and finally direct *on-crystal* micro- and macro-structuring [2, 11]. The first two approaches unfortunately did not yield any useful results. This is seen in the crystal's intrinsically broad angular light spread at the exit of the scintillator [2,11,12]. Simulations of the on-crystal micro and macro-structuring, however, gave very promising results (Figs. 9, 10).

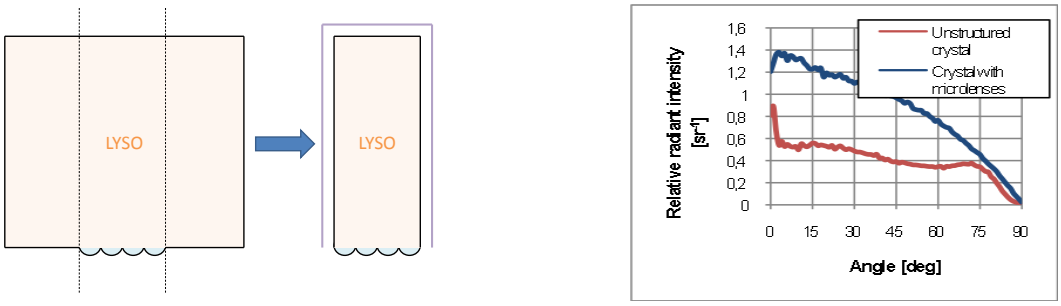

Fig. 9: Schematic of the Micro-lens light extractor

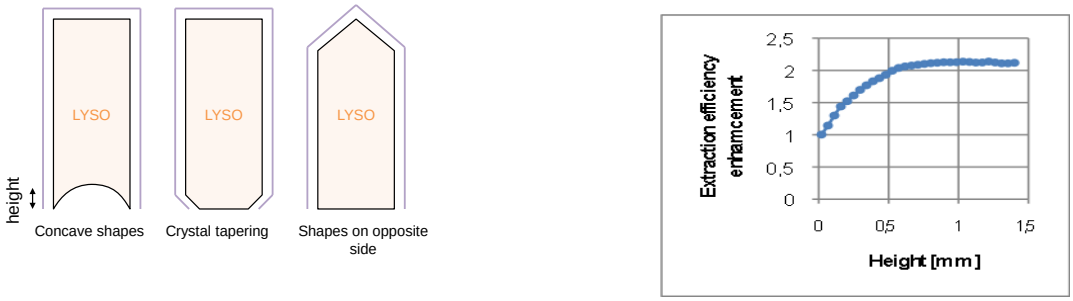

Figure 10: Geometric examples of direct on-crystal macro-structuring (left). Simulated increase in light extraction efficiency in air with a concave crystal (right).

The company Kloé, member of the consortium, developed a dedicated lithography protocol for micro-structuring to "write" micro- structures or -patterns directly on the crystal surface. Figs. 11, 12 illustrate the result of this method tested on a glass cube. The same technique is currently being applied on a LYSO sample to assess the expected gain in LY.

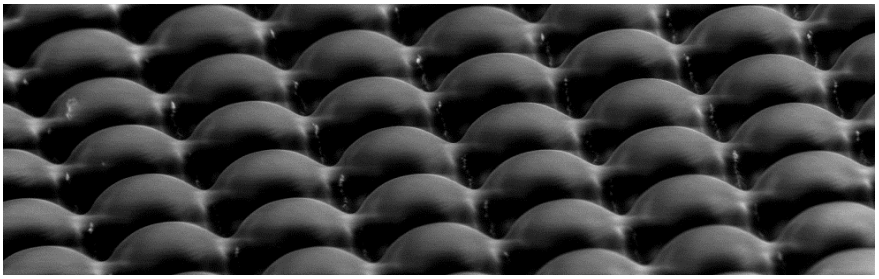

Figure 11 : SEM image of the micro-lenses "engraved" on a glass cube surface

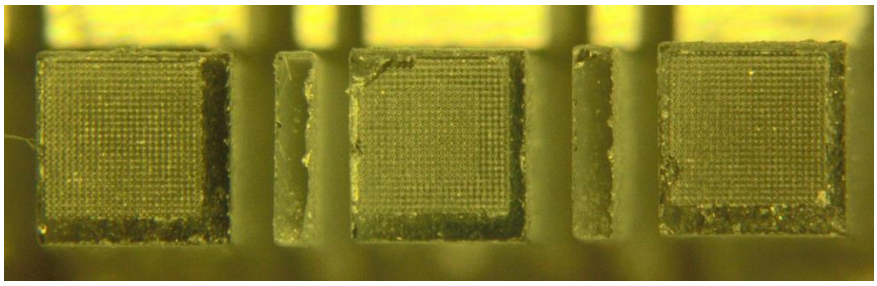

Figure 12 : Micro-lens matrices on a glass cube after cutting

For the macro-structuring, preliminary experimental results show a gain up to 30% in light collection [13]. However, further investigations are still needed before this technique can be applied.

Since, at this time, still no satisfactory optical element capable to increase the required optical gain could be identified, and since macro-structuring is still felt not to be safe enough to be applied on a full crystal matrix, it was decided that the crystal matrix for the first prototype of the internal probe be glued directly on the *digital* SiPM. In view of the fact, though, that the measured LY of the crystals turned out to be nearly two times higher than foreseen, enough light is produced so that one can cope with the absence of an optical concentrator.

References:

[1] E. Auffray et al, "A comprehensive & systematic study of coincidence time resolution and light yield using scintillators of different size, wrapping and doping¨, IEEE NSS/MIC, 2011 IEEE, pp. 64 – 71, November 2011 and Nuclear Science, IEEE Trans. Nucl. Sciences, Vol. 60, 2013, pp 3163 - 3171

[2] Technical report M1-M18, WP2 activities

[3] S. Farah and al., Growth and Characterization of Ce:LuAG Fibers Developed by the µ-pulling-down Technique, presented at the SCINT2015 conference

[4] Marie Skłodowska-Curie R&I Staff Exchange (RISE project) Intelum, Grant agreement no: 644260

[5] E. Auffray et al, "Design and performance of detector modules for the endoscopic PET probe for the FP7-project EndoTOFPET-US", Nuclear Science Symposium and Medical Imaging Conference (NSS/MIC), 2012 IEEE, pp3236-3240

[6] 3M, Vikuiti Enhanced Specular Reflector (ESR); http://multimedia.3m.com/mws/mediawebserver?mwsId=66666UuZjcFSLXTtMxMyOXM6EVuQEcuZgVs6EVs6E666666--&fn=ESR%20ss2.pdf

[7] Z. Liu et al., "Quality control of the TSV multi-pixel photon counter arrays, and modules for the external plate of EndoTOF-PET ultrasound detector", Nuclear Instrumentsand Methods in Physics Research A787(2015)240–244

[8] E. Auffray et al, "Characterization studies of silicon photomultipliers and crystals matrices for a novel time of flight PET detector", 2015 JINST 10 P06009 doi:10.1088/1748-0221/10/06/P06009

[9] F. Anghinolfi et al., "NINO: An Ultrafast Low-Power Front-End Amplifier Discriminator for the Time-of-Flight Detector in the ALICE Experiment" IEEE Trans. Nucl. Sci., vol. 51, No. 5, pp. 1974-1978, October 2004.

[10] V1290A-2eSST, 32-Channel Multi-hit TDC. www.caen.it.

[11] Technical report M19-M36, WP2 activities

[12] G. Fornaro et al, Study of the Angular Distribution of Scintillation Photons, proceeding of SCINT2013 conference, Nuclear Science, IEEE Transaction, 2013, pp1-6

[13] M. Nemallapudi et al, "Alternative geometries for improved light output of inorganic scintillating crystals", presented to SCINT2015 conference

WP3: Photodetectors

The new generation of digital photodetectors developed in this project is the central component of the endoscopic probe. Because, it has to meet the challenging requirements regarding timing resolution and miniaturization. The name of the new generation digital silicon photomultiplier is array of 9x18 Multichannel Digital Silicon Photomultipliers (MD-SiPMs).

The endoscopic PET detector module, is composed of two arrays of 9x18 MD-SiPMs, required circuitry to operate the sensors, and two matrices of 9x18 LYSO pixels. Since the detector will be placed inside the probe, all of the functionality must be miniaturized. Consequently, the array of 9x18 MD-SiPMs is a monolithic system-on-chip that features time-to-digital converters (TDCs), high dark-count-rate (DCR) masking circuits, energy thresholds, readout system, etc. In addition, the printed-circuit-board (PCB) that contains the die includes a field programmable gate array (FPGA). The interfacing between the DAQ system of the EndoTOFPET-US and the arrays of 9x18 MD-SiPMs is performed by the low-power and small-footprint FPGA.

A detailed block diagram of the array of 9x18 MD-SiPMs is shown in Fig. 1. It consists of 9×18 cluster array, column circuits, a row decoder, a read/write (R/W) register, a reference voltage generator, and direct outputs multiplexer. Timing data lines and energy data lines are shared by column SPAD cells. Thus, in total, 48 timing data lines are routed out from 18 clusters, even though 48 timing data lines are dedicated for one cluster during the gamma detection since it is assumed that scintillations occur in one cluster only for each frame of 6μs. The energy data is read out by selecting the row of interest. Each of the 432 timing data lines (48 data lines per cluster column, 9 cluster columns) is equipped with column circuits, comprising signal buffers and reset circuitry, Mask registers, energy calculators, and a column-parallel TDC. A dead-time-less reset mechanism called smart reset is used to filter spurious events that have insufficient radiation energy.

Upon detection of a possible gamma event, its energy is estimated in the Energy Calculator, which scans all clusters that have the highest numbers of fired SPAD cells in each cluster column employing the fast energy readout system. The mask register is used for disabling those SPAD cells with DCR exceeding a threshold, so as to minimize spurious TDC activation. The column-parallel TDC acquires timestamps of photons produced by a scintillator to estimate Time of Arrival (TOA) of the shower generated by the gamma photon. The reference circuit is implemented for biasing the column-parallel TDC. The R/W register is used for controlling the cluster array chip and for correcting the data to be read out outside the chip. The timing data of clusters are also routed to input/output (I/O) pads via a direct multiplexer for testing purposes. One cluster column (48 timing data lines) is selected out of 9 cluster columns by the configuration memory. The array of 9x18 MD-SiPMs is fabricated with a 0.35 μm high-voltage CMOS process.

The size of the chip is 7.6 mm × 17.1 mm. Each cluster in the array comprises 416 SPAD cells, and measures 800×780 $\mu m^{2,}$ adapted to the crystal dimensions. A 20 μm gap enables adequate glue reflow in the pixelation process. Each SPAD cell measures 50 μm×30 μm. In the cell, the SPAD is implemented along with cell circuitry as shown in the microphotograph in Fig. 2.

After the design and implementation stages of the array of 9x18 MD-SiPMs, the system-on-chip was fully measured and verified. The full characterization included electrical verification and testing, as well a radiation measurement.

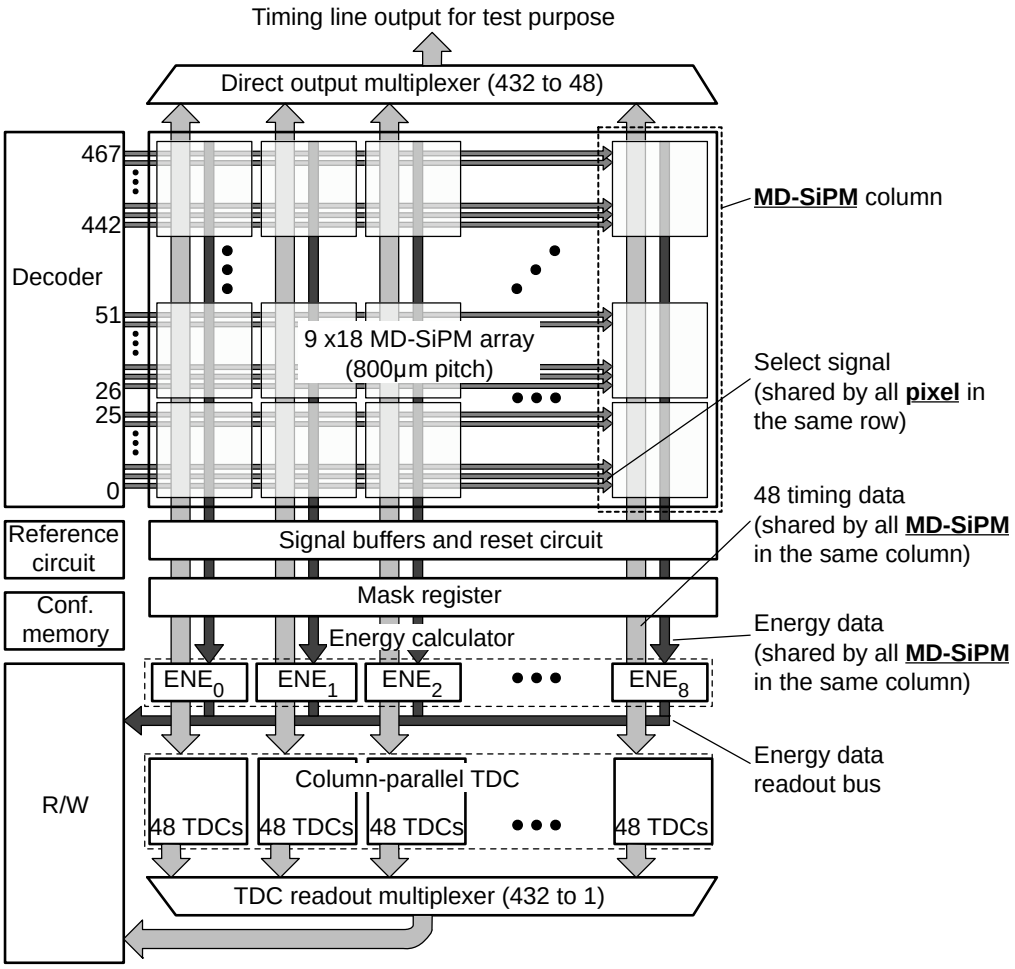

Fig. 1 : Detailed functional block diagram of the array of 9x18 Multichannel Digital Silicon Photomultipliers.

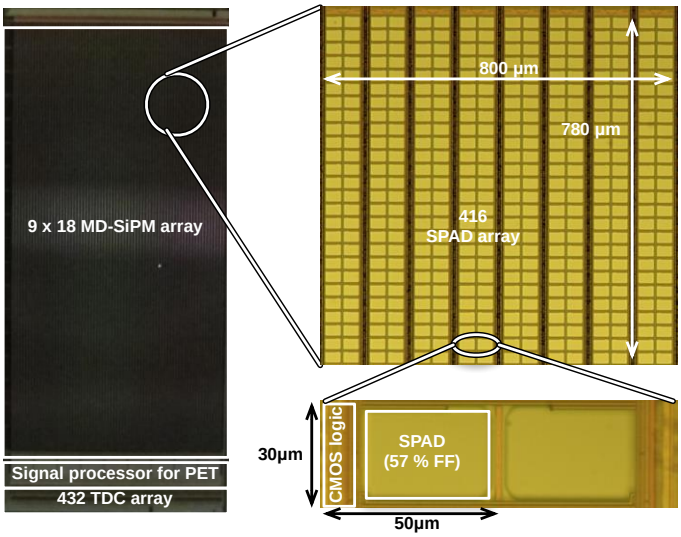

Fig. 2 : Array of 9x18 Multichannel Digital Silicon Photomultipliers microphotograph.

Table 1 summarizes the measurement results of array of 9x18 MD-SiPMs and compares them to the original specifications. The array of 9x18 MD-SiPMs features optimized SPAD cell circuits and an

embedded smart reset; that is a circuit that only resets the TDCs triggered in the previous detection cycle.

Table 1. *Summary of the array of 9x18 MD-SiPMs features and comparison with original specs.*

Parameter		Original spec	Measurement of 4x4 array	Measurement of 9x18 array
Chip	# cluster	9 x 18	4 x 4	9 x 18
	# SPAD / cluster	416	416	416
	Pitch cluster (µm)	800	800	800
	Reset scheme	-	Smart reset (60ns)	Smart reset (< 20ns)
TDC	# TDCs / cluster column	32	48	48
	TDC accuracy	50	50	49.5
SPAD	DCR (Hz/µm^2)	15	50	50
	PDP (%)	35	30	30
	Jitter (ps)	64	104	104
	FF (%)	50	57 (D15)	57 (D15)
	Afterpulsing prob. (%)	5	0 (1bit CNT)	0 (1bit CNT)
SiPM (416 SPADs)	PDE (%)	-	< 17	< 17
	Total DCR (MHz)	0.5	> 1	> 1
	Cross-talk (%)	15	< 10	< 1.8
	Screamer (%)	5	< 20	< 20
	STR for single photon (ps)	-	200	200-320

The chip was characterized with the DAQ board built by one member of the consortium in Portugal (LIP) in order to test the communication link and integration to the final system. A Dark Count Rate (DCR) measurement on the latest version of the chip was carried out. The chips were characterized in DCR and compared to previous versions. For this operation all the SPAD cells were activated and the DCR was measured over several seconds at room temperature. Fig. 3 shows an example of the DCR map of the entire array of 9x18 MD-SiPMs.

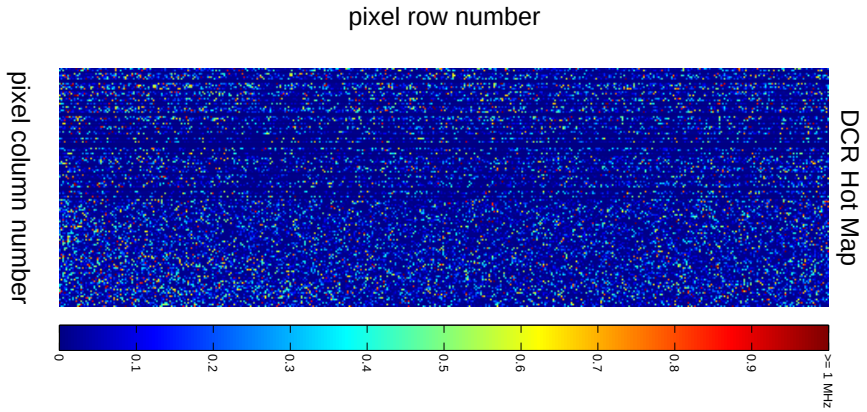

Figure 3. Dark count rate measured on entire active area of the array of 9x18 MD-SiPMs.

The high dark-count-rate (DCR) suppressor circuit called masking circuit was also characterized. This circuit is present in every SPAD cell of the array of 9x18 MD-SiPMs and deactivates the higher DCR cells. Fig. 4 shows the DCR map of the detector when deactivating a percentage of the total SPADs cells starting from the more noisy to the less noisy cells.

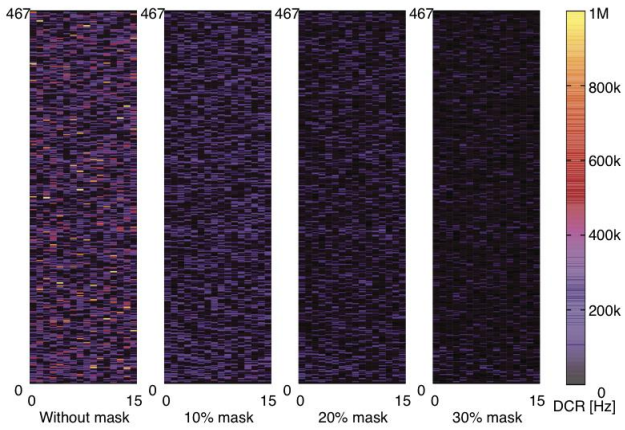

Fig. 4: Masking effects in a column of chip .

In addition, a radiation characterization was performed. We chose a scintillator size of 3x3x10mm^3 in order to have a considerable gamma count rate in the scintillator. The LYSO pixel size was 3x3x10mm^3 and we utilized a ^{22}Na radioactive source of 300µCi.

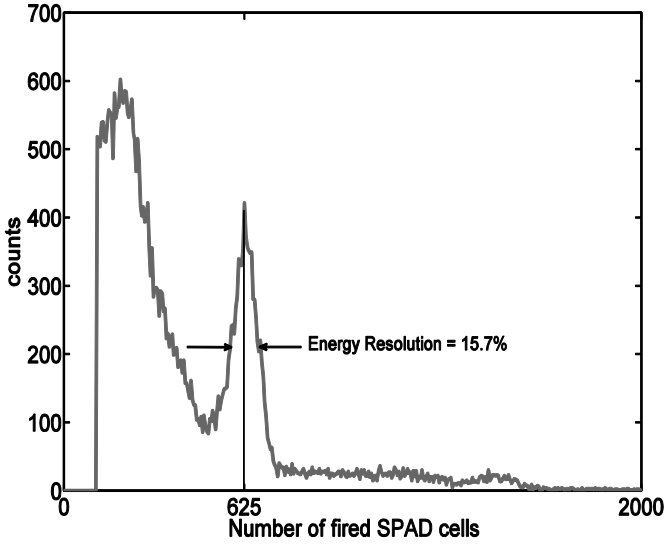

Fig. 5: Energy Spectrum of ^{22}Na.

In summary, the architecture of multichannel digital SiPM was introduced, developed and implemented. The obtained performance was compatible with the original specifications of the EndoTOFPET-US probe detector. The system was fully designed, implemented, verified and characterized.

WP4 : Front End (FE) and Data Acquisition (DAQ) electronics

The main objectives of the Work Package 4 (WP4) were to develop low noise and fast SiPM readout and data acquisition electronics for the external pates of the EndoTOFPET-US imaging systems (prostate and pancreatic systems). This work package was under the responsibility of LIP-Lisbon. The University of Heidelberg, DESY and CERN were also involved in the development.

The front-end electronics for the external PET plate involved different developments and tasks. It included:

- The development of two front-end ASICs allowing to readout 64 SiPM channels, including time stamping and energy measurements, suitable for PET Time-of-Flight (TOF);
- The development of the frontend electronics boards housing the ASICs and providing the DAQ interface links, as well as clock and control links.
- The development of the trigger and data acquisition system, integrating data links from the internal probe and from the external PET plate.

In order to reduce the technological risk, two designs of the front-end TOF ASIC allowing to readout 64 SiPM channels were pursued. While the conceptual design and interface specifications are the same in both developments, two different TDC designs were pursued, one based on digital phase-locked loop and another based on analog integration and time amplification. The first development (by University of Heidelberg) used silicon technology UMC 180 nm, and the second (by LIP-Lisbon) used technology IBM 130 nm. CERN and DESY provided technical support and advise to both projects.

a) TOF ASIC: development by University of Heidelberg

The final version of the readout chip (STiC3) was designed at the Kirchhoff-Institute for Physics (KIP) in Heidelberg. This chip is a 64-channel readout ASIC in UMC 0.18 μm CMOS technology. The time and charge information of the input signal is converted into two time stamps which are digitized by an integrated TDC with a time binning of 50 ps. A special linearized Time-over-Threshold method has been implemented to provide a linear response to the signal charge over a wide range. The digitized event information is stored in a FIFO memory and transmitted every 6.4 μs to an external DAQ system using a 160 MBit/s LVDS serial link with 8/10-bit encoding. Fig. 1 shows a picture of the chip wire-bonded to the PCB board.

The electronics jitter of less than 20 ps for signals with more than 3 pixels firing has been measured using its analog front-end. In addition, a coincidence timing resolution (CTR) of 214 ps has been measured using the EndoToFPET US detector modules consisting of $3.1\times3.1\times15$ mm^3 LSO cystals and 3×3 mm^2 MPPCs (Hamamatsu S10362-33-50C), see Fig 2. The outstanding performance of the linearized Time-over-Threshold method is proven by ^{22}Na energy spectra obtained with this chip (Fig. 3): the 0.511 MeV and the 1.27 MeV photo-peaks are clearly visible in the spectrum. Finally, using more recent detector modules providing higher light yield, a CTR of less than 200 ps has been achieved.

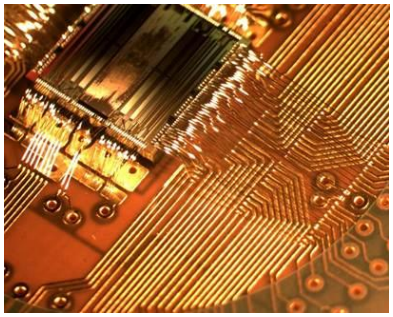

Fig. 1: STiC3 wire-bonded to the PCB

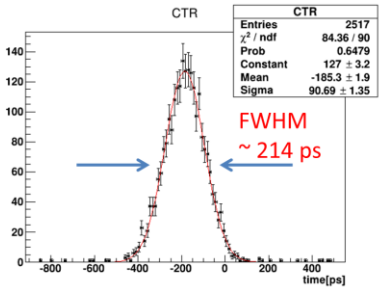

Fig. 2: Coincidence Timing Resolution (CTR) of the Na^{22} source

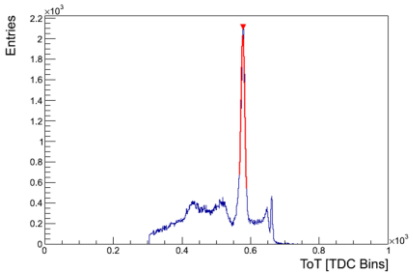

Fig. 3: Energy Spectrum of the Na^{22} source

b) TOF ASIC: development by LIP-Lisbon

The 64-channel TOFPET chip was developed at LIP Lisbon in CMOS 130 nm technology (Fig. 4). The measurements of the S-curve (counting rate as a function of threshold) close to the baseline indicate a sigma of noise of 2.6 mV, which matches the simulated value for a SiPM terminal capacitance of 300 pF. The pulse amplitude for a single-photon is around 30 mV. The signal shape at the input of discriminator was evaluated: the measured slew rate of the rising edge of 511 keV event pulses is 500 mV/ns.

The baseline setting was measured to have an excursion of 500 mV allowing fine tuning of the SiPM bias voltages. The total average power consumption is 8.0-11.0 mW p/channel depending on the chip configuration.

Time measurements were performed with MPPCs arrays of discrete TSV type. For laser measurements, a precise laser (PicoQuant Laser) generating 420 nm light pulses impinging directly on MPPC pixels was used. For CTR measurement, LYSO crystals of 3.1x3.1x15mm^2 have been used. The chip was configured with TDC binning of 50 ps. The channel rate in CTR measurements (Na22 source) was around 4 kHz. Laser pulse rate was 80 kHz. The Time Resolution measured laser pulses was 32 ps r.m.s. (Fig. 5). The CTR measured with a Na22 source was 272ps FWHM (Fig. 6).

The full-chip, running at 160 MHz, was tested with internal data generator up to 6.4 MHz (100 kHz/channel), well above the rate estimation in the EndoTOFPET external plate, which is 10 kHz/channel.

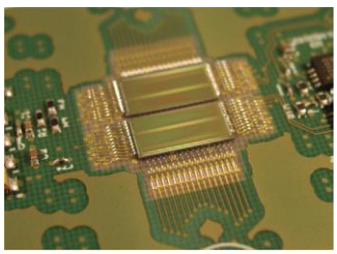

Fig. 4: TOFPET chips wire bonded in the frontend board

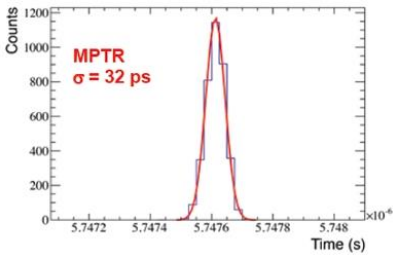

Fig. 5: Time resolution measured with laser pulses.

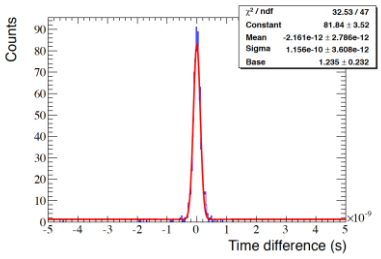

Fig. 6: Coincidence Time Resolution measured with LYSO crystals (FWHM=270 ps).

c) External plate FEB/A Boards: development by LIP-Lisbon and Univ. of Heidelberg

The frontend system comprises physically two types of boards, the board housing the ASICs (FEB/A) and the board interfacing to DAQ (FEB/D). The ASICs are wire bonded directly to the FEB/A Printed Circuit Board (PCB). Two types of FEB/A board have been developed: STiC and TOFPET versions (see Fig. 7 and 8).

The FEB/A has one connector for each MPPC matrix allowing for easy replacement of damaged components. The connectors between the FEB/A daughter boards and the FEB/D motherboard provide connections for input voltages, MPPC bias voltages, clocks, control bus and output links. The boards FEB/A and FEB/D are mounted in opposite sides of the cooling plate. The FEB connectors traverse the cooling plate though appropriate holes.

The FEB/A STiC is used in the external plate of the prostate system. A multi-chip module (MCM) has been designed to serve as an accustomed package for the STiC3 chip. Two MCMs are BGA-soldered onto one FEB/A boar, which is used as a front-end readout module for the external plate. A flex PCB extension providing space for the decoupling capacitors assembles the STIC chip in a module formed by a double-layer PCB (Fig. 7). The achieved STiC3 channel yield for the prostate system was 99%.

The FEB/A TOFPET board has also modularity of 128 channels housing two 64-channel TOFPET ASICs, and has approximate dimensions of 3x6 cm. The TOFPET chips are assembled in a single-layer PCB version of the FEB/A (Fig. 8). MPPC connectors are mounted in the board back side.

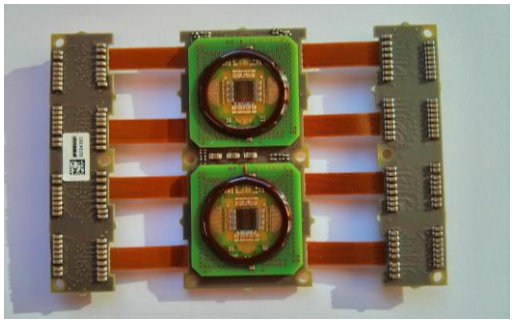

Fig. 7: One STiC electronics module (128 channels), two MCMs BGA-soldered on the FEBA board

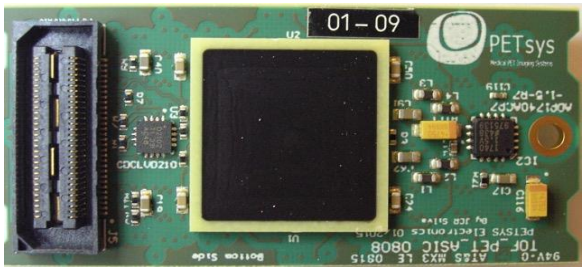

Fig. 8: The TOFPET FEB/A board with 128 channels (two ASICs under the common globtop protection epoxy.

d) External plate FEB/D Boards and DAQ electronics: development by LIP-Lisbon

The FEB/D has modularity of 4x2 FEB/A, and the total number of FEB/D boards in an external PET plate is four, each with approximate dimensions of 12x12 cm (Fig. 9).

The FEB/D boards can be integrated with the DAQ board forming a complete scalable data acquisition system with several thousand channels. The EndoTOFPET system has 4096 channels. Each FEB/D board collects the data of 1024 channels and transmits assembled data frames through an electrical serial link (1.6 Gbps) of two high-speed optical links (2x6.4 Gb/s). Using the optical links, the maximum output event rate per FEB/D is 128 M event/s (full event format) or 256 M events/s (compact event format).

On board DC-DC converters provide all voltages need to operate the full system using a single external power supply of 12-24 V. On board SiPM bias voltage regulation (64 lines) are also available. The FEB/D board is equipped with a Kintex 7 FPGA which contains the firmware needed to configure the frontend ASICs and to read the data.

The DAQ backend is implemented in PCI-e board interfacing directly to the DAQ computer (Fig. 10). It includes a powerful Virtex FPGA suitable to implement the trigger and data acquisition firmware. Four high-speed links to the external plate and up to two links to the endoscopic probe are available on the DAQ board. Links for control and configuration of the frontend systems are also implemented, as well as central distribution of clock and sync signals.

The high-speed communication and data transfer between the front-end and the back-end DAQ system is implemented by complex firmware running in FPGAs in the both ends. The firmware is responsible to move data from the external plate ASICs and from the endoscopic probe system up to the data acquisition computer.

Fig. 9: The FEB/D board.

Fig. 10: The DAQ board.

WP5: Detector integration

Work Package 5 (WP5), dedicated to the integration, has provided the support and coordination to integrate all detector and software components of the project.

a) Mechanical Design and Assembly

On the mechanical side, an extension for an existing Hitachi trans-rectal ultrasound probe was designed to combine it with an encapsulated miniaturized PET probe for endoscopic use. Fig. 1a shows two MPPC arrays coupled to two LYSO crystals matrices of 16 crystals each, read out via a TOFPET chip hosted on a dedicated PCB board, which provides the communication to the DAQ. This PET probe is encapsulated and fixed to the ultrasound probe (shown on Fig. 1b). The design includes copper pipes for the circulating water cooling of the electronics.

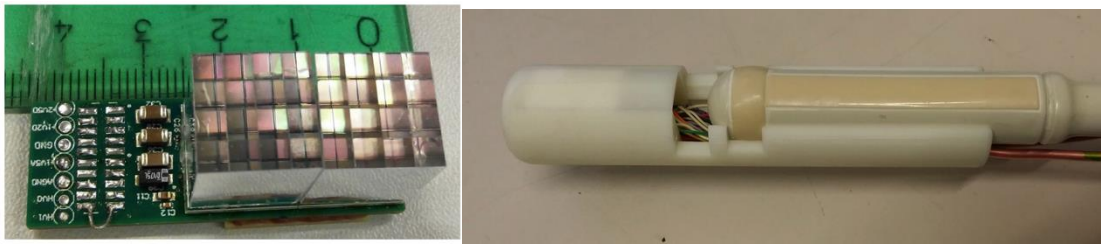

Fig. 1 a) The intermediate PET head detector featuring two crystal matrices glued on Hamamatsu MPPC matrices, connected to the PCB hosting the TOFPET chip for the MPPCs readout and the electronics for the communication with the DAQ. b) Encapsulated PET head detector mounted on the Hitachi ultrasound probe.

The external detector is a plate hosting 4096 individual channels (Fig. 2b). Each channel is a LYSO crystal of 3x3x15 mm^3 in size coupled to a MPPC photo-detector from Hamamatsu. The MPPCs are mounted on a dedicated flexible PCB hosting the readout chip (STiC v3.0) that is named FEB-A (Front End Board – Analog), shown in Fig. 2a. The FEB-As are mounted on the DAQ interface card (called FEB-D, Front End Boards - Digital). In between the FEB-As and theFEB-D a cooling plate ensure sufficient water flow to remove the heat dissipated by the electronics.

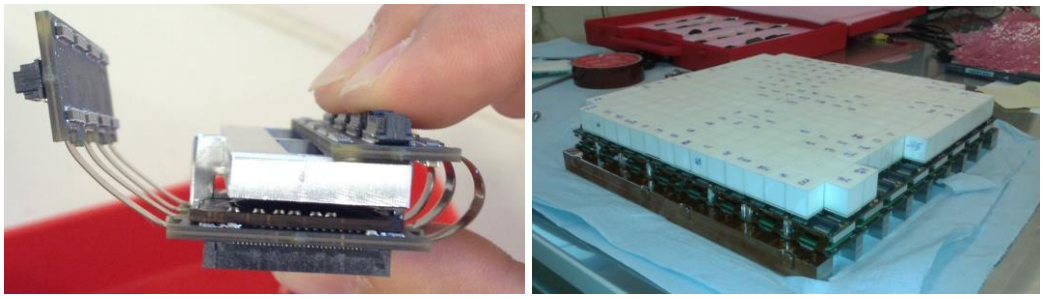

Fig.2 a) The flexible PCB hosting STiC v3.0 two readout chips. b) the assembled crystals and photodetectors on the cooling plate of the external detector.

After the characterization of all components, the integration and the assembly of the first external plate started in autumn 2014 at DESY.

A special mechanical housing that ensures the fixation of all crystals and electronics was mounted (Fig. 3). It also hosts the cooling system and provides light tightness. The cooling system was thoroughly tested for leakage, and a smoking test of the electronics was performed before shipping the detector to CERN for commissioning.

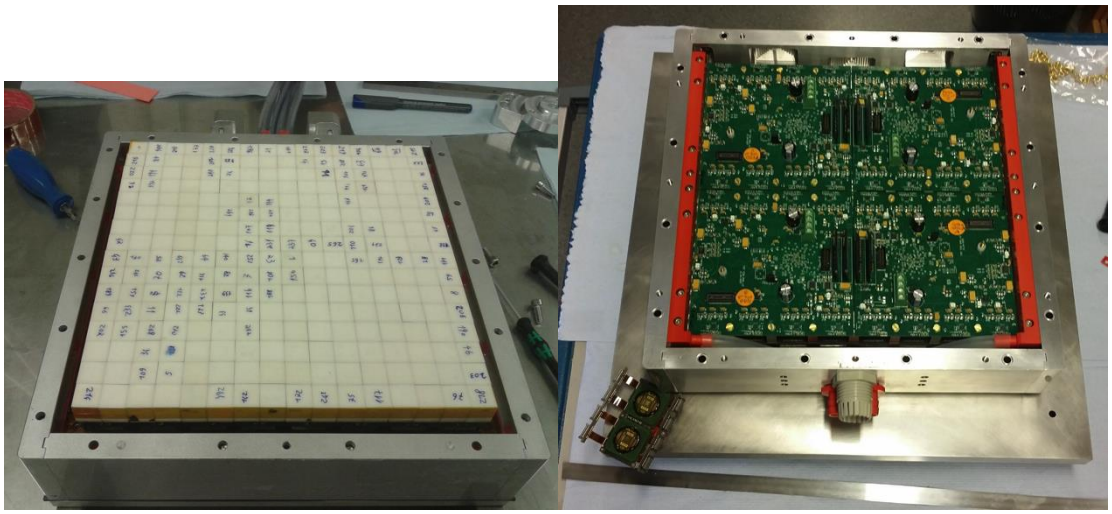

Fig. 3 a) top view of the open external plate. Visible are the crystal matrices assembled on the electronics. b) bottom view of the open external plate. Visible is the electronic PCB board and in red the sidewalls of the cooling system.

b) Integration and test of the complete detector.

The STiC v3.0 and the TOFPET chip were successfully integrated in the DAQ readout and data was acquired with the coincidences between the external plate and the provisional internal probe detectors. The energy response of all available channels was calibrated with a β+ emitting source, in order to evaluate the detector response for the 511 keV gammas of the positron annihilation. The data have been synchronized such that coincidences from a point-like source placed between the two detectors could be obtained.

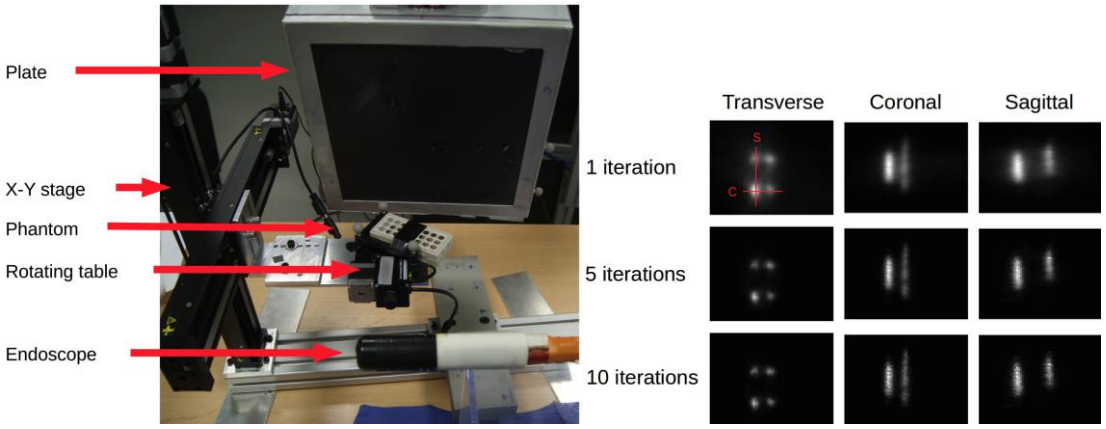

Fig. 4 a) Test setup for the detector integration and calibration. b) Image reconstruction of data acquired with the EndoTOFPET-US detector, showing transverse, sagittal and coronal views of a phantom of 4 cylinders. The image quality improves with increasing iterations of the MLEM

algorithm. The red lines show where the sagittal and coronal views have been acquired.

Finally, the system was prepared for the pre-clinical tests: the external plate was mounted on a movable arm attached to a movable cart, where all the necessary equipment (chiller, power supply unit, DAQ PC, cables) are stored. Moreover, a slow control was developed in order to facilitate the usage of the device. It also provides a continuous monitoring of all the system components, preventing severe damages in case of single failures. The position of the detectors is tracked using a commercial optical tracking system Polaris Vicra from NDI.

The preclinical tests were performed at CERIMED, Marseille (Fig. 4a). First PET images of few phantoms filled with FDG have been achieved, proving the feasibility of the free-hand PET system (Fig. 4b). A promising spatial resolution of the order of a millimeter was obtained, with static detectors. Only minor deterioration of the image is obtained in the free-hand mode of operation, i.e. moving the endoscope with respect to the fixed external plate.

c) Development of simulation and reconstruction software to optimize the detector design and study its performance

A full simulation framework, based on existing extensions for emission tomography of the Geant4 Monte Carlo particle simulation code such as GATE and GAMOS was developed to evaluate detector performance and image quality as a function of different detector configurations. It pays attention to the proper use of time-of-flight (TOF) information. Loading of voxelised DICOM data allows for the incorporation of attenuation and activity data from real PET/CT scans. The simulations are designed to run on computing clusters.

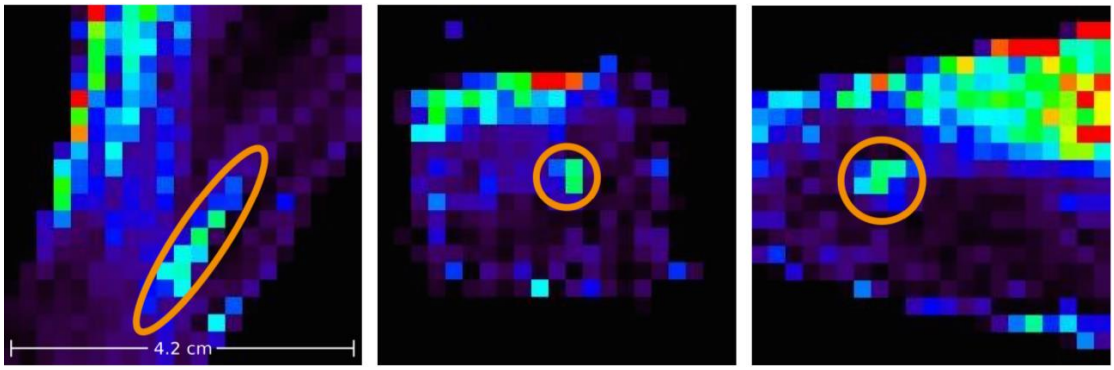

Fig.5 Reconstructed image from a simulated EndoTOFPET-US acquisition based on PET/CT data of patient with prostate lesion tagged with PCa. The lesion (circled in the transverse, sagittal and coronal views) is visible and separated from the bladder, which gives the remaining uptake in the image.

Studies with varying acquisition time and detector movements show that a scan time of approximately 10 min and small rotation of around 10 degrees yields sufficient image quality. The use of high-resolution full-body patient as phantoms suggests that the endoscopic approach of the EndoTOFPET-US detector is able to separate the prostatic lesion well from the background radiation from prostate and bladder (Fig. 5).

The reconstruction algorithm masters the difficulties arising from performing a free-hand acquisition with a system that has low sensitivity. It benefits from an implementation on graphics processing units (GPU) for parallelized execution. It is further improved and corrected based on the results of whole-body simulations. Its validity is further confirmed by reconstruction of data that is acquired during the commissioning phase.

d) Development of a high precision referencing system for the relative alignment of inner and outer PET detectors and magnetic field test.

The EndoTOFPET-US detectors can be tracked with an optical tracking system or with a hybrid approach combining optical with electromagnetic tracking.

We developed, in collaboration with clinical partners, a framework for the acquisition, fusion and visualization of data from the nuclear detector, the ultrasound machine and the tracking system. It is designed as an open-source multimodal image-guided system for endoscopic organ biopsy and tested on whole-body PET/MR data that is registered to live interventional ultrasound images. This approach aims at providing a research platform that can be used, beyond EndoTOFPET-US, for the implementation and rapid translation into clinical use of new image segmentation, registration and visualisation approaches (Fig. 6).

The technical user interface is based on TANGO, a framework for building distributed heterogeneous control systems.

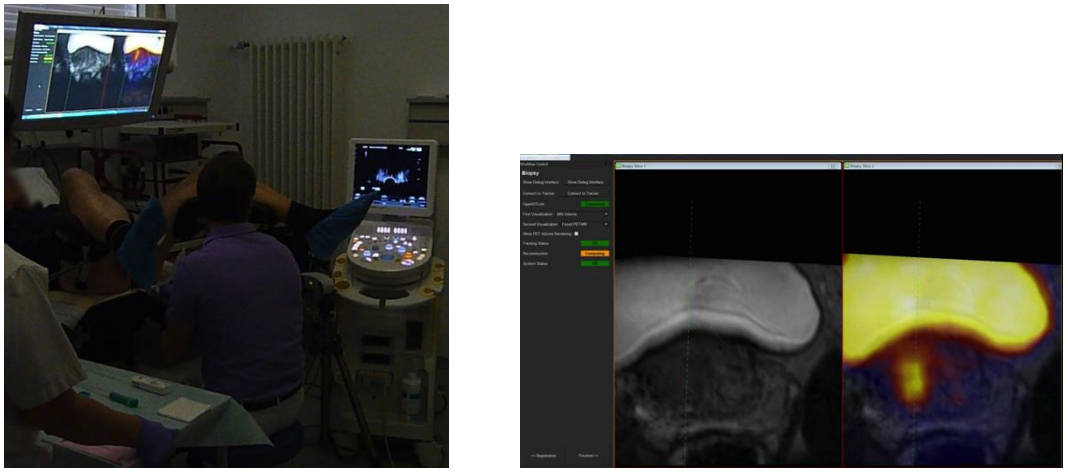

Fig. 6 a) picture of the graphic user interface (GUI) provided for the EndoTOFPET-US project, in use for a PET/MR to TRUS fusion image-guided prostate biopsy. b) Snapshot of the GUI.

WP6: Clinical requirements & preclinical and pilot clinical studies

The main results from Workpackage 6 can be divided under 3 categories.

a) **Clinical requirement, indications and protocols**

The first task in the project was to gather t different specifications towards the clinical oriented development of the EndoTOFPET-US system. This information, based on the human anatomy, international standards, cleaning procedures and medical examinations, was opportunely shared with the technical partners of the consortium, mainly to Workpackage 5, to ensure an application-suitable design and implementation of the device.

The outer dimensions of the probe are limited not only by the organs and structures surrounding the area of examination, but also by the characteristics of the path inside the body that the probe needs to overcome to arrive to the area of interest. The maximum dimensions of the pancreatic probe (diameter and rigid part length) are limited by the anatomical characteristics of the upper gastrointestinal tract. The tightest part is the upper esophageal constriction, behind the hyoid bone (lingual bone), with a diameter of 12-14 mm. The maximum length of the rigid tip is determined by the sharp curve when passing from the stomach through the pylorus to the duodenum and should not exceed 50 mm. For the prostate scenario, the gland lies at a low level in the lesser pelvis, anterior to rectourethralis muscle and the rectal ampulla, through which it may be palpated and examined with a transrectal probe. These anatomical constraints allow the probe to have a larger diameter of even 25 mm and set no practical constraints regarding length or rigidity.

Endoscopes are usually cleaned and high-level disinfected mainly using an automatic device similar to a dishwasher, which uses a combination of special detergents and disinfectants containing peracetic acid and hydrogen peroxide. The temperature varies between 35°C and 40°C during the disinfection stage and reaches up to 67°C for the drying process. For some interventions a lubricant containing Lidocaine (local anaesthetic) is applied to the inserting portion of the endoscope. Transrectal probes are covered during the examination with a latex sheath, on top of which a specific US-Gel is applied. The probe is cleaned only using an Isopropanol-based cleaner and isn't exposed to high temperatures.

Regarding the operational constraints of the EndoTOFPET-US device for the foreseen applications, the International Electrotechnical Commission (IEC) defines the standards for medical electrical equipment and the maximum admissible values of temperature (endoscopic 41°C, extern 43°C), current (patient leakage 100μA) and voltage ("floating" ground, 42.4V (peak, AC) or 60V (DC)). The international guidelines for personnel exposure to radiation during the operation of the developed device have been studied and related to the EndoTOFPET-US project by comparison to previous studies found in literature. The International Commission on Radiological Protection (ICRP) sets a limit for the annual occupational exposure for adults of 20 Millisievert (mSv) of effective dose over one calendar year, considering the average over a 5 year-period (100 mSv in 5 years) and a total effective dose equivalent below 50 mSv in any single year. Due to the configuration of the EndoTOFPET-US device, the personnel exposure can be estimated by comparison to that of radio-guided surgeries. Based on this, the exposure due to the operation of the developed device would remain well below the allowed limits, allowing one physician to perform a large number of interventions in a calendar year. The radiation exposure is monitored during the trials, to ensure the compliance with these norms for a future certification of the device.

The workflow of the medical procedures of interest for the EndoTOFPET-US system has been established through visits to routine examinations of both pancreas and prostate patients. For an endosonographic examination of the pancreas, the lightly sedated patient lies on her or his left side. An assistant supports the physician during the whole procedure, which normally lasts 30 to 40 minutes. In the case of a prostate examination, superficial US and digital rectal inspections precede the transrectal US procedure. The completely awake patient lies on one side, and the entire examination lasts less than 10 minutes, the transrectal exploration about 3 minutes. The position of the patient during both examinations could be changed to ensure a practicable geometrical configuration between the external plate, the internal probe and the anatomic region of interest. The only exception is in the pancreas examination, where the patient can't lie on his right side to avoid suffocation. The space available in these operation rooms allows placing all the needed hardware of the EndoTOFPET-US system with no need for major modifications.

An anonymous database of over 850 PET/CT and PET/MRI examinations on patients has been created, selected according to the diagnosis of not only pancreas and prostate cases, but also from other pathologies whose examination might benefit from the EndoTOFPET-US system. A study has been performed extracting anatomic and metabolic parameters from patients that underwent an ^{18}F-FCH PET/CT, indicated for the initial diagnosis of prostate cancer, as well as from ^{68}Ga-PSMA PET/MRI examinations performed in patients with histologically confirmed prostate cancer without prostatectomy. The study contains detailed clinically relevant anatomic (e.g., volume of prostate, bladder and lesions), metabolic (e.g., average tracer-uptake in the organs (background) and lesions) and examination-related (e.g., injected activity) information, which has been provided to the simulation and image reconstruction team of Workpackage 5.

An investigation has been carried out of the key regulatory aspects towards a possible future application of the EndoTOFPET-US device in humans and contact to this end has been already established with the relevant Swiss national authorities (SwissMedic MD, Cantonal Ethics Comission). The urology and surgery departments of the project's medical partners have already shown their willingness to participate in the realization of clinical trials as soon as the device will be fully operational and clinically applicable.

b) Monitoring, development and selection of biomarkers

The selection of biomarkers suitable to use in combination with the EndoTOFPET-US system was the second task of WP6. The non-invasive multimodal endoscopic probes designed in this project will be used to track the radiotracers targeting specific tumoral prostatic and pancreatic biomarkers.

To improve the diagnosis of pancreatic adenocarcinoma (PDAC) compared to the standard PET radiotracer (^{18}F-FDG), more specific and more sensitive new biomarkers have been identified to evaluate their potential use for PDAC imaging. Two commercially available antibodies against pancreatic biomarkers, Mesothelin and CEACAM5 (Carcino-Embryonic Antigen related Cell Adhesion Molecule 5), have been selected to be conjugated to a PET radionuclide for PDAC imaging. The mAb16D10 monoclonal antibody against a tumoral glycoform of the Bile Salt-Dependent Lipase (BSDL) expressed in pancreatic cancer has been developed. In collaboration with Roche Glycart, a therapeutic humanized 16D10 IgG form of mAb16D10 has been created. Currently, the establishment of a new collaboration contract with Roche Glycart is ongoing to test this humanized antibody in PDAC imaging on animal models and further in human diagnosis. The

biomarker S100A7 (Sporiasin) has been described for the first time in PDAC by using MALDI Imaging Mass Spectrometry and in-source decay (Proteomic Platform - CRO2). The expression of S100A7 was validated by immunohistochemistry on SOJ-6 xenografted tumors and on human pancreatic tissues.

To allow the application in cancer PET imaging, the conjugation of antibodies against the selected biomarkers to a linker DOTA and a PET radiotracer such as ^{68}Ga is being performed in collaboration with Professor B. Guillet (CERIMED). Within the same collaboration, the use of biomarkers for imaging and detection of pancreatic neuro-endocrine tumors (PNET) with the EndoTOFPET-US system is pursued. First assays have been performed with ^{111}In-DOTATATE or ^{68}Ga-DOTATATE (a somatostatin analog used in nuclear medicine PNET imaging) to detect xenografted AR-42J tumors on nude mice by using small animal SPECT or PET scanners, respectively.

As soon as the EndoTOFPET-US systems allows it, the described newly characterized biomarkers will be validated by using pig models of pancreatic cancer. For the first EndoTOFPET-US prototype, developed as a prostate oriented device, it is possible to use the PET radiotracers ^{11}C-Choline, ^{18}F-Choline, ^{68}Ga-Bombesin and ^{68}Ga-PSMA to detect prostatic cancer in animal models with implanted human-tumor cells. The choline-based radiotracers are the gold-standard for PET prostate examinations, while both ^{68}Ga-labelled compounds have been recently developed and are currently facing different stages towards their incorporation into clinical routine.

The development of ^{68}Ga-NODAGA-MJ9 (Bombesin) for prostate cancer (as well as ^{68}Ga-NODAGA-RGD for different types of cancer including pancreatic cancer) has led to its first use in human as part of a wide clinical research protocol. The ongoing study consists in multimodal PET/CT imaging of prostate carcinoma (PCa) patients with known primary cancer before prostatectomy as well as in patients with a suspicion of recurrence after prostatectomy. Each patient undergoes a standard ^{18}F-Choline PET/CT followed by a ^{68}Ga-NODAGA-MJ9 PET/CT examination, allowing for direct comparison between both radiotracers in PCa imaging.

^{68}Ga-PSMA is a recently developed PET radiotracer for prostate cancer that, compared to the gold-standard choline tracers, performs better at low PSA (prostate-specific antigen) blood values, has a higher uptake by PCa lesions and a low background signal. This results in an improved detection of PCa relapse and metastasis, allowing the detection of small lymph node, bone and liver metastases. In the nuclear medicine department of one EndoTOFPET-US medical partner, all ^{11}C-Choline prostate PET examinations have been replaced by the use of ^{68}Ga-PSMA. In addition to the diagnostic benefits, the longer half-life of ^{68}Ga (68 minutes) compared to ^{11}C (20 minutes) allows injecting a much lower radioactive dose, reducing thus the exposure of both patients and personnel.

Once the EndoTOFPET-US device is ready for its clinical use, the trials can be performed using both novel ^{68}Ga-NODAGA and ^{68}Ga-PSMA radiotracers at the nuclear medicine departments of the project's medical partners.

c) Implementation of a preclinical evaluation of the EndoTOFPET-US system on pigs

This task refers to 1) the preclinical evaluation of the device itself, as provided by the other WPs, and 2) the settlement of experimental models of cancerous lesions relevant to the human situations in order to reproduce the pathologic behaviour of the tumours (It should be kept in mind that nuclear medicine is based upon peculiar, abnormal fixation of radionuclides by cancerous tissues).

The first endocavitary EndoTOFPET-US probe delivered to the preclinical team was a designed on the basis of a combination of the specific requirements derived from the clinical practice and the technical realities of the device. It revealed difficulties in its practical implementation because it folded at the US-PET junction. Other problems were recognized, such as the position of the spatial tracking system on the probe's grip hindering the handling of the device, a too large diameter and water leakage. By the end of the three periods of trials, the probe has been redesigned with an improved rigidity, reorganizing of the wires and blinding of the probe, as shown in the left image of the Fig. 1. Under various imaging procedures based on the routine human practice, the probe has proven to be advanced and placed at the appropriate sites in anesthetized animals.

Fig. 1: Left) Optimized final version of the EndoTOFPET-US probe. The probe was found to be usable under the clinical practice for prostatic investigations and clinicians approved the design of the prototype. The probe was optimally placed in-situ according the ultrasonic imaging of the prostate. Right) Arrangement of the whole EndoTOFPET-US system within a standard examination room.

The following step was to manage the organization of the complete EndoTOFPET-US system in the reality of the PET-scanner's room, which enables the "control" visualization of the lesions under the common, sophisticated instrument, as in the clinics. In the right image of Fig. 1, from right to left are: the computer cart enabling both the acquisition and treatment of data from the external plate and the in-situ probe; the pig laying on the table of the discovery 710 (128 slices, GE) with the probe placed for the examination; the AVIUS Hitachi US echograph controlling the US probe that is coupled to the PET-head; the control US echograph for external US investigations; the 3D optical-tracking-camera which identifies the spatial positioning of the probe. This equipment arrangement enables the EndoTOFPET-US imaging procedures and concomitantly the traditional PET-scan and US echographic imaging, in order to control the results.

To manage the implantations of primary human carcinoma (Kc), a great effort has been paid to inhibit the porcine hyper-active immune rejection of the grafted Kc. Similarly, the multiple problems of tumors implantation were finally managed, so that experimental models were validated with human cancerous tumors growing in the prostate or in the pancreas of the pigs.

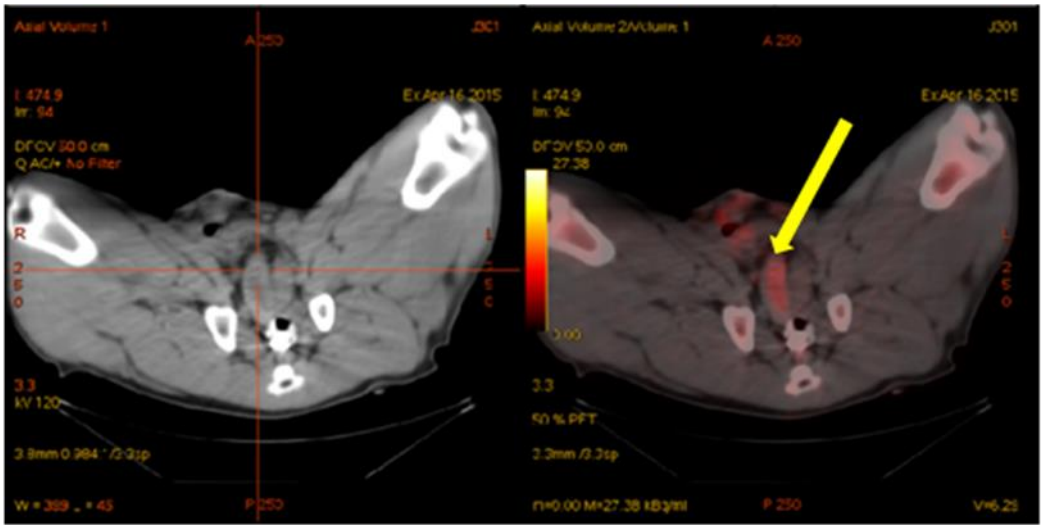

Fig. 2 :PET/CT image of a succesfully implanted and grown human prostate carcinoma in a pig.

The following step was to confirm that the implanted Kc elicited an identical behavior by using the reference radionuclide (^{18}FDG, ^{18}F-Choline and attempts with ^{68}Ga-PSMA). Fig. 2 illustrate the ^{18}F-Choline labeling of a prostatic tumor in right prostatic lobe (note the very weak labeling of the left lobe), the small dot on the right of the labeled lobe was proved to be an extra-lobe masse of the tumor.

As a conclusion the developed EndoTOFPET-US probe has been proved to be able to investigate prostate lesions in pigs. Prostate and pancreas cancers were successfully implanted in the appropriate organs that are relevant to the human situations. Finally, the lesions were identified by using state-of-the-art PET investigations.

It has been decided to pursue the program in applied phases because the major developments have been done to the probe and detection systems. Therefore, the pilot clinical evaluation of the EndoTOFPET-US system is foreseen to happen within a follow-up project, once the system has been furhter tested and optimized with both laboratory (phantoms) and preclinical trials.

4.1.4 Impact of the project

In contrast to state-of-the-art endoscopic imaging, which provides structural and in the best case superficial functional information with a limited sensitivity the EndoTOFPET-US probe includes the possibility of obtaining high sensitivity functional information during endoscopy, which is (a) specific (i.e. is based on specific biomarkers) and (b) goes beyond the walls of the examined lumen.

The detection limit of commercial PET scanners is at the level of 0.3-1 cm^3. The EndoTOFPET-US probe can detect tumors of less than 10 mm^3 with a localization and definition of tumor margins in 3 dimensions with a precision of about 1 mm.

Furthermore the EndoTOFPET-US probe, with a timing resolution of 200 ps, will allow defining a Region of Interest of 3 cm diameter, improving the signal to noise (S/N) ratio by a factor 3 to 10 and allowing new and faster reconstruction methods to be implemented. Operation of the probe with a possible dose reduction can therefore be expected and will be investigated in further exploitation of the system.

All these technological advances have a high impact on a number of domains:

1. On medical procedures:

Minimally invasive surgery (NOTES, SILS and therapeutic endoscopy) will gain from new procedures created by introducing novel endoscopic tools allowing performing image-guided interventions based on PET functional imaging superimposed with ultrasound anatomical image. The field of therapeutic oncology will ultimately benefit from improved ability to successfully and more rapidly obtain tissue material during biopsies or to help tumour resection with an unprecedented definition of tumour margins during either surgery or endoscopy. This project, with its preclinical validation phase and it strong clinical focus from the beginning of the project and throughout the whole development phase will provide the necessary input to launch carefully planned clinical studies on several highly selected clinical applications on specific cancers or inflammatory diseases, in view of a fast routine clinical exploitation of its results.

A high impact is expected in the understanding of tumour biology and physiopathology: this approach will allow improving actual tumour biology markers and participate to the development of new biological markers. The introduction of high specific PET biomarkers for early cancer detection is constrained due to low resolution of clinical PET scanners (partial volume effect, etc.). The EndoTOFPET-US probe will enable high specific PET biomarkers accumulating in very small structures to be easily distinguished from the background. This will allow simplified and faster validation of new biomarkers. In particular, thanks to the improved sensitivity, biomarkers trapped by and into lesions will be better studied than currently possible through the unprecedented performances of the probe and would improve understanding of physio-pathological phenomenon such as malignant metastasis or early response. This would benefit to the development of newer biomarkers allowing a correlation of the imaging characteristics to the histo-pathological response thanks to tissue samples obtained with this new EndoTOFPET-US probe.

Tumor entities like pancreatic and prostatic cancer are asymptomatic commonly with poor prognosis (like in the case of pancreatic cancer) and invasive surgical treatment. The EndoTOFPET-US probe will allow less invasive and more precise micro-surgical interventions, as well as validating new diagnosis protocols based on newly developed and more specific biomarkers, which could further result in an improvement of the prognosis in malignancies like pancreatic cancer.

Higher precision in drug targeting is also expected through the development of specific biomarkers and the ability to detect them early in the carcinogenesis thanks to the endoTOFPET probe. This approach could be applied to new therapeutic modalities on very small lesions with a possible follow up of the clinical response with the same technology. One can concieve that when a drug is attached to the biomarker it can selectively act on the specific target, while other tissue are much less altered by the drug.

Hadrontherapy will also indirectly benefit from the outcome of the project. On-line monitoring of dose distribution during proton or carbon therapy treatment requires very high sensitivity, high resolution and fast reconstruction imaging of β^+ emitting isotopes produced by beam or target spallation processes during the irradiation. Only TOF-PET with timing resolution in the few hundreds ps range and direct 3D reconstruction algorithms can achieve this very challenging goal.

2. On patients

The most important impact is allowing easier procedures to achieve detection of small, early lesions: this will allow more precise and early diagnosis and possible treatment of primitive or secondary tumours by improving visualisation of tissue, biopsies or more complete resections of tumours. Higher sensitivity and image quality will allow detecting smaller tumours or tumour residues participating ***to improving diagnosis, treatment and thus survival***, as well as faster exams, contributing to ***improved patient comfort.***

Another important impact is on a significant dose reduction, scaling like the improvement of the S/N ratio introduced by TOF techniques, which will directly benefit the patients and the medical personnel in the intervention room. Moreover fast reconstruction and improved image quality will allow a quick feedback about the exam and contribute to ***less patient recall*** (e.g. multiple biopsies for prostate or pancreatic cancer).

3. On health care costs

Minimally invasive surgery guided by cutting edge imaging techniques and surgical endoscopy have a high cost reduction potential through shorter hospitalization or even outpatient setting, and reduced complication rate such as adhesions or infections, decreased surgical stress/postoperative inflammation and less immuno-suppression. The proposed project further extends the domain of procedures available during minimally invasive surgery with the ability to more easily and faster obtain tissue sample as well as to allow better surgical or endoscopic resection of tumours. This could translate in being able to diagnose disease much earlier than actual methods, at a stage where it is much easier to treat and to cure. This has an enormous potential for health care costs and intangible costs that are more difficult to quantify.

More generally TOF-PET techniques allow a reduction by one order of magnitude on the time of the exam to reach an equivalent image quality than with conventional non TOF PET scanners. Pushing the TOF performance to the limit will bring a ***significant improvement on the patient throughput per machine and reduce the overall cost of the exam.***

4. On medical technology and other domains than medical

The technology developed in this project can readily be transposed and employed for the design of conventional PET/CT. Many advantages would come from this technology, as it would be able to withstand very high magnetic fields allowing ***its use in the next generation of hybrid PET/magnetic resonance imaging (PET/MR) hybrid scanners***. Moreover, such detector would be able to detect a very large energy range and work as well as to detect X-rays used in CT part of the PET/CT. Miniaturized high performance TOF probes will find applications in several other domains than medical. ***The proposed technological breakthrough in sensitivity and image quality should allow better performance and higher throughput in domains such as homeland security (luggage screening, non-proliferation of fissile materials) and industrial non-destructive testing and quality control of complex structures.***

It will also help ***improving detectors in fundamental sciences*** such as particle and nuclear physics.

5. On European industry

European industry, and in particular SME's are looking for possibilities to integrate cutting edge technology they are developing into final products, and to demonstrate the added value of their implementation in these products. The EndoTOFPET-US project involves 3 SME's working in different domains such as scintillating heavy crystalline fibre production, diffractive optics and innovative integrated computer-aided solutions for surgical procedures. As such it provides a unique opportunity to introduce these companies on a segment of the medical market, which has high revenue potential, and to take lead positions through the combination of their technologies.

4.1.5 Public website address and relevant contact details

- **Website:** http://endotofpet-us.web.cern.ch/endotofpet-us/

- **Project Management Team :**
  -Project coordinator: René Laugier (AMU), rlaugier@ap-hm.fr
  -Project technical coordinator: Paul Lecoq (CERN), paul.lecoq@cern.ch
  -Project Manager: Johanna Kabadanian (AMU/Protisvalor), johanna.kabadanian@univ-amu.fr

- **Principal Investigators in each partner institution:**

Beneficiary 1, Coordinator : Aix-Marseille University (AMU):

1. Team 1a. AMU/AP-HM (René Laugier, rlaugier@ap-hm.fr)
2. Team 1b. AMU/Cerimed (Pierre-Henri Rolland, pierre-henri.rolland@univ-amu.fr)
3. Team 1c. AMU/CRO2 (Eric Mas eric.mas@univ-amu.fr, Dominique Lombardo dominique.LOMBARDO@univ-amu.fr)

Beneficiary 2 : European Organisation for Nuclear Research (CERN) (Paul Lecoq paul.lecoq@cern.ch, Etiennette Auffray etiennette.auffray@cern.ch),

Beneficiary 3 : Centre Hospitalier Universitaire Vaudois et Universite de Lausanne (CHUV-UNIL) (John Prior, John.Prior@chuv.ch , Claudio Bruschini, claudio.bruschini@epfl.ch)

Beneficiary 4 : Deutsches Elektronen-Synchrotron (DESY), (Natalia Potylitsina-Kube, natalia.potylitsina-kube@desy.de)

Beneficiary 5 : Delft Technical University (DELFT TU) (Edoardo Charbon, e.charbon@tudelft.nl)

Beneficiary 6 : Fibercryst (Jean-Marie Fourmigue jm.fourmigue@fibercryst.com)

Beneficiary 7 : Kloe SA (KLOE) (Paul Coudray, coudray@kloe.fr)

Beneficiary : Laboratorio de Instrumentacao e Fisica Experimental de Particulas (LIP) (Joao Varela, joao.varela@cern.ch)

Beneficiary 9: SurgicEye GmbH (Thomas Wendler wendler@surgiceye.com, Joerg Traub, traub@surgiceye.com)

Beneficiary 10 : Technische Universitat Munchen (TUM) (Benjamin Frish, benjamin.frisch@tum.de Nassir Navab, navab@cs.tum.edu)

Beneficiary 11 : University of Heidelberg (UHEI) (Hans-Christian Schultz- Coulon, coulon@kip.uni-heidelberg.de)

Beneficiary 12: University Milano Biccoca (Unimib) (Marco Paganoni, marco.paganoni@cern.ch)

Beneficiary 13: Klinikum Rechts der Isar der Technischen Universitat Munchen (TUM-MED) (Markus Schwaiger, markus.schwaiger@tum.de Ian Schweiger Somlai, ian.somlai@tum.de)

Beneficiary 15: University of Hamburg (Erika Garutti, erika.garutti@physik.uni-hamburg.de)